Available online at www.sciencedirect.com

ScienceDirect

Advances in Space Research 70 (2022) 3686–3698

ADVANCES IN SPACE RESEARCH (a COSPAR publication)

www.elsevier.com/locate/asr

Investigations of equatorial plasma bubbles as observed in the OI 630 nm nightglow emissions over off-equatorial and low-latitudinal locations over Indian longitudes

Sovan Saha [a,b], Duggirala Pallamraju [a,*], Rupesh N. Ghodpage [c]

[a] *Physical Research Laboratory, Ahmedabad, India*
[b] *Indian Institute of Technology, Gandhinagar, India*
[c] *Medium Frequency Radar Facility, Indian Institute of Geomagnetism, Shivaji University Campus, Kolhapur, India*

Received 3 April 2022; received in revised form 8 July 2022; accepted 7 August 2022
Available online 11 August 2022

Abstract

Equatorial plasma bubbles (EPBs), generated over the dip-equator during the sunset time, get mapped over to the low-latitudes through the geomagnetic field lines and contribute to structures of different scales in the nighttime thermosphere-ionosphere system. In the present study, the EPBs are observed in the OI 630 nm nightglow emissions over Mt. Abu and Kolhapur using a High Throughput Imaging Echelle spectrograph (HiTIES) and All-Sky Imager (ASI), respectively. Similar periodicities obtained in these measurements consistently corroborate the presence of the EPBs at both these locations. The strength of the Pre-Reversal Enhancement (PRE) in the zonal electric field has been investigated using the ionosonde data over Trivandrum, a dip-equatorial location. The strength of PRE decides the latitudinal extent of the EPBs. The eastward movement of the EPBs has been estimated to be in the range of 190–90 ms^{-1}, decreasing in magnitude from post-sunset to midnight. The wave number analysis carried out using the observed OI 630 nm emissions in the zonal direction has resulted in a contrasting behaviour during the presence/absence of the EPBs. Based on the analysis of around 1300 images of data, it is revealed that the scale sizes in the range of 250–300 km are omnipresent, whereas, shorter scale sizes (50–250 km) are present only during the presence of EPBs. It is inferred that these shorter scale size gravity waves played a significant role in the seeding the perturbation of the EPBs.

Keywords: OI 630 nm nightglow; Equatorial plasma bubbles; Equatorial electrodynamics; Gravity waves; Ionosphere-thermosphere system; High-resolution spectrographs

1. Introduction

Equatorial ionospheric irregularities can extend to large spatial distances in latitudes, which pose significant adverse impacts on trans-ionospheric radio wave propagation during their presence. The GPS receiver shows scintillations in the signals due to loss in phase locks. This brings practical difficulties in navigation and satellite-based communication, and so it motivates the scientific community working in the ionospheric studies to understand these phenomena in greater detail. The sharp plasma density gradient in the ionospheric F-region altitudes during sunset time sets the stage for the onset of ionospheric irregularities. These irregularities span a wide range of scale sizes from a few centimetres to several thousand kilometres, as observed in different techniques. Some of the manifestations of these irregularities are the spread in reflected echoes (spread-F) of radio frequency as seen in ionograms, plasma bubbles as seen in optical imagers, plasma plumes as observed using radars,

* Corresponding author.

https://doi.org/10.1016/j.asr.2022.08.023
0273-1177/

and plasma scintillations as seen in VHF and GPS measurements (e.g., Farley et al., 1970; Woodman and La Hoz, 1976; Abdu et al., 1983; Kelley, 1985; Takahashi et al., 2001, 2021; Huang et al., 2013; Patra et al., 2014; Abadi et al., 2015; Huang and Roddy, 2016; Sivakandan et al., 2019; Takahashi et al., 2021). Generalised Rayleigh-Taylor instability (RTI) generates the bubble-like structures, which, to the first order, are understood to be responsible for the generation of such plasma irregularities over the magnetic equator (Balsley et al., 1972; Kelley, 1985). The RTI growth rate is dependent on the magnitude and the sense of the equatorial eastward electric field and neutral winds, gravitational force, ion-neutral collision frequency, electron density gradient, and vertically downward winds, among other factors (Haerendel et al., 1992; Kelley, 1985; Sekar and Raghavarao, 1987; Sultan, 1996). Numerous investigations have been carried out, which brought out several important aspects/factors with regard to this plasma irregularity formation and morphology. Some of them that play a significant role in the generation and growth of the plasma instability are: the strength of equatorial ionization anomaly (EIA) in the daytime (e.g., Kelley, 1985; Raghavarao et al., 1988; Sridharan et al., 1994; Pallamraju et al., 2004; Prakash et al., 2009), the pre-reversal enhancement in the electric field, field-line integrated conductivity of the medium (Abdu et al., 1982; Tsunoda et al., 1985), neutral winds (both vertical and meridional), (Maruyama and Matuura, 1984; Sekar and Raghavarao, 1987; Raghavarao et al., 1987, 1993) and gravity waves (GWs) (Kelley et al., 1981; Kelley and Hysell, 1991; Abdu et al., 2009). Modelling studies have evolved over the decades to understand the linear, non-linear growth of plasma bubbles, the effect of the electric field, and winds in the generation and growth of plasma bubbles (e.g., Ossakow, 1981; Sekar and Raghavarao, 1987; Haerendel et al., 1992, Sekar et al., 1994, 2001; Sultan, 1996; Huba et al., 2008; Krall et al., 2009). In parallel, observational studies have been carried out using ground-based and satellite-borne measurements (e.g., Tsunoda et al., 1982; Kil et al., 2009; Karan et al., 2020; Park et al.,2022), which increased our understanding of the plasma instabilities, and their structure, and zonal drifts.

Optical emissions have been used extensively in the investigations of equatorial plasma bubbles (EPBs). OI 630.0 nm and 777.4 nm emissions originating from around 250 km and peak F-layer, respectively, are more commonly used for the investigations of EPBs (Mendillo and Baumgardner, 1982; Kelley et al., 2002; Makela and Kelley, 2003; Mukherjee et al., 2003; Rajesh et al., 2010; Sekar et al., 2012; Ghodpage et al., 2014) as the electron densities play an important role in the production of these emissions. The plasma bubbles which are generated over the dip-equator rise to higher altitudes in response to the eastward electric fields and come down to the low-latitudes along the geomagnetic field lines due to ambipolar diffusion and pressure gradient forces. The apex altitudes to which the bubbles reach can be as high as 1700 km. These plasma bubbles are aligned along the magnetic field lines as demonstrated by the simultaneous observation from two geomagnetic conjugate locations (e.g., Otsuka et al., 2002; Shiokawa et al., 2004), wherein, the structures of the plasma bubbles and their bifurcations at the conjugate locations do match fairly well with one another. Several characteristics of the plasma bubbles, like, westward tilt of the bubble structures and eastward movements, have been investigated from different longitude sectors (Mendillo and Tyler, 1983; Makela and Kelley, 2003; Mukherjee et al., 2003; Pimenta et al., 2001; Sekar et al., 2012; Ghodpage et al., 2014; Gurav et al., 2019; Karan et al., 2020). The neutral wind measurement using the Fabry-Perot interferometer over the Brazilian sector had been shown to match very well with the zonal plasma drift as well as with the zonal drift of plasma bubbles (Chapagain et al., 2012, 2013).

In this study, we present the results obtained from observations of OI 630 nm nocturnal emissions carried out during January to March in the year of 2014 from two different locations, namely, Mt. Abu (24.6°N, 72.7°E, 19°N Mag) and Kolhapur (16.8°N, 74.2°E, 10.4°N Mag). Mt. Abu is typically located at the northern edge of the EIA crest, whereas, Kolhapur is located between the magnetic equator and the northern crest of the EIA. Signature of the plasma bubble has been observed in the OI 630 nm emissions from these two locations using two different optical instruments, High throughput Imaging Echelle Spectrograph (HiTIES) over Mt. Abu and All-sky Imager (ASI) over Kolhapur. This passive remote sensing of the upper atmosphere has resulted in improving our understanding of the signatures of nighttime GW behaviour both in zonal and meridional directions. The plasma bubbles are clearly seen as depletions in emissions in the imager and the spectrograph. The zonal plasma drift, horizontal scale sizes as obtained from the imager data, and the plasma bubble periodicity obtained from two locations will be discussed in detail.

2. Observations and data used

2.1. OI 630 nm nightglow emissions

The OI 630 nm airglow emissions originate at an altitude centred at 250 km with around 100 km full-width half maxima during nighttime. The nighttime OI 630 nm emission is produced following a two-step mechanism. Firstly, the O^+ charge exchanges with O_2 to produce O_2^+. Then the dissociative recombination of O_2^+ produces excited atomic oxygen ($O(^1D)$) in the presence of background thermal electrons, which, on the transition to the ground state, releases 630 nm photons. This forbidden state of $O(^1D)$ has radiative lifetime of 110 sec, so it has enough time to equilibrate with the thermospheric dynamics. Thus, the OI 630 nm nightglow emission variation provides information on the thermospheric-ionospheric interaction and enables investigations of the upper atmospheric dynamics.

2.1.1. HiTIES observations

HiTIES is a high spectral resolution slit spectrograph (Chakrabarti et al., 2001) which is in operation from Mt. Abu, India. HiTIES has a spectral resolution of 0.06 nm at 630 nm. It uses 1024 × 1024 pixels CCD which are binned 1 × 16 in the spatial direction, to improve the signal-to-noise ratio. The field-of-view (FOV) of HiTIES is around 54° along the slit, which is oriented in the geomagnetic north–south direction for this experiment. The data cadence is 5 min. Dark count, vignetting effects, and Van Rhijn effects have been considered in the images before further analyses are carried out. Greater information on the instrument, its working, and data processing has been reported in earlier works (Chakrabarti et al., 2001, Saha et al., 2021).

2.1.2. All-sky imager observation

The data set from an all-sky imager located at an off-equatorial station, Kolhapur, is used in this study. The 1024 × 1024 pixels CCD-based ASI gives 140° FOV, which covers around 1200 km distance (Sharma et al., 2014). To avoid the curvature and non-linear effects that exist in the image at larger incident angles, we have taken around 100° FOV, which corresponds to around 600 km horizontal distance both in the zonal and meridional directions in our analysis. Around 20 nights of clear sky (cloud-free) data have been obtained during the period Jan to Feb in the year 2014.

2.2. Digisonde

Radio-sounding data using Digisonde Portable Sounder (DPS-4D) from two locations Trivandrum (8.5°N, 76.9°E, 0.03°N Mag) (dip equatorial location) and Ahmedabad (23.0°N, 72.6°E, 17.3°N Mag) (a low-latitude location) have been used in this study. The digisonde provides the ionospheric information every 7.5 min. During the presence of plasma irregularities, spread in reflected radio echoes are seen in the ionograms rendering the measurement of the height of the F-region ambiguous. Therefore, during the absence of spread-F and until the occurrence of spread-F, we have estimated the plasma drifts over the equator. Further, in order to avoid uncertainty in the estimation of plasma drifts which can arise due to the recombination in the bottom side of the F-region (Bittencourt and Abdu, 1981), we have used 7 MHz isoelectron density contours, which are typically above 300 km, to calculate the sunset time F-layer vertical drift over the dip-equator.

3. Observations and results

Different types of variability in the OI 630 nm nightglow emissions have been observed from a low-latitude location, Mt. Abu. After the sunset, as the electrons recombine rapidly, OI 630 nm emissions decrease monotonically from 18:45 LT, when the HiTIES observations begin in a programmed mode (Fig. 1a). The different colours represent emissions that originate from different directions as viewed from HiTIES, as mentioned in this figure. On several nights, we have observed an enhancement in emissions after around 1.5 h of local sunset (Fig. 1b) at around 21 LT. A poleward meridional wind which brings down the plasma to the 630 nm emission altitudes, has been found to be the cause of such emission enhancements (Saha et al., 2021). Apart from that, we have observed excursions in emissions on some nights (as shown in Fig. 1c, d). There are four depletions in emissions that have been observed on 26 Feb 2014 at 20:30, 21:25, 22:45, and 24:35 LT (Fig. 1c). A close inspection indicates that the emissions decrease at the same time and with the same magnitudes in all directions, north, zenith and south at 21:25 LT. Whereas, for the other depletions, the southern side emissions (dashed blue line) show a much sharper and deeper decrease than that on the northern side. Similarly, the depletions in emissions seen on the other night, 05 Mar 2014, have different rates of decrease in different directions. All these differences are the tell-tale signature of the plasma bubbles, their latitudinal and longitudinal extents, etc., as will be clear once the data from other datasets are presented and discussed as given below. Out of 68 moonless clear sky nights during Jan-Mar of the year 2014, 26 nights showed such sudden depletions in emissions.

The simultaneous digisonde measurement from nearby location in Ahmedabad indicated the presence of spread-F in the ionogram during the times of depletions in the nightglow emissions observed from Mt. Abu. These locations of spread-F are indicated with the shaded region (pink coloured horizontal lines) in Fig. 1c and 1d. It should be mentioned here that the other two nights in Fig. 1a and 1b are non-spread-F nights. The presence of spread-F at the time of depletions in emissions suggests the presence of strong plasma irregularities over this region. The presence of depletions in emissions over Mt. Abu coincides on all (100 %) of the occasions with the spread-F seen over Ahmedabad, indicating the extent of large-scale size plasma irregularities at least until 19° magnetic latitude on those nights. However, only on 69 % nights of spread-F observations over Ahmedabad coincides with the occurrence of plasma depletion over Mt. Abu, which indicates that the bubbles did not extend beyond 17° magnetic latitude on 31 % of nights.

To ascertain that such sharp fluctuations as obtained in our measurements over Mt. Abu are due to plasma depletions, we have also investigated the OI 630 nm all-sky images obtained from Kolhapur, which is situated between the magnetic equator (Trivandrum) and low-latitude region (Mt. Abu/ Ahmedabad). We have around 20 clear nights of data from the imager during the same period of Jan-Mar in the year of 2014. Fig. 2 shows OI 630 nm nightglow variation from both the places, Mt. Abu and Kolhapur. The meridional segment (12 km over zenith × 600 km along south-north) from each of the images obtained from Kolhapur is arranged with time to form a keogram and is shown in the bottom panels of the Fig. 2. In the top panels,

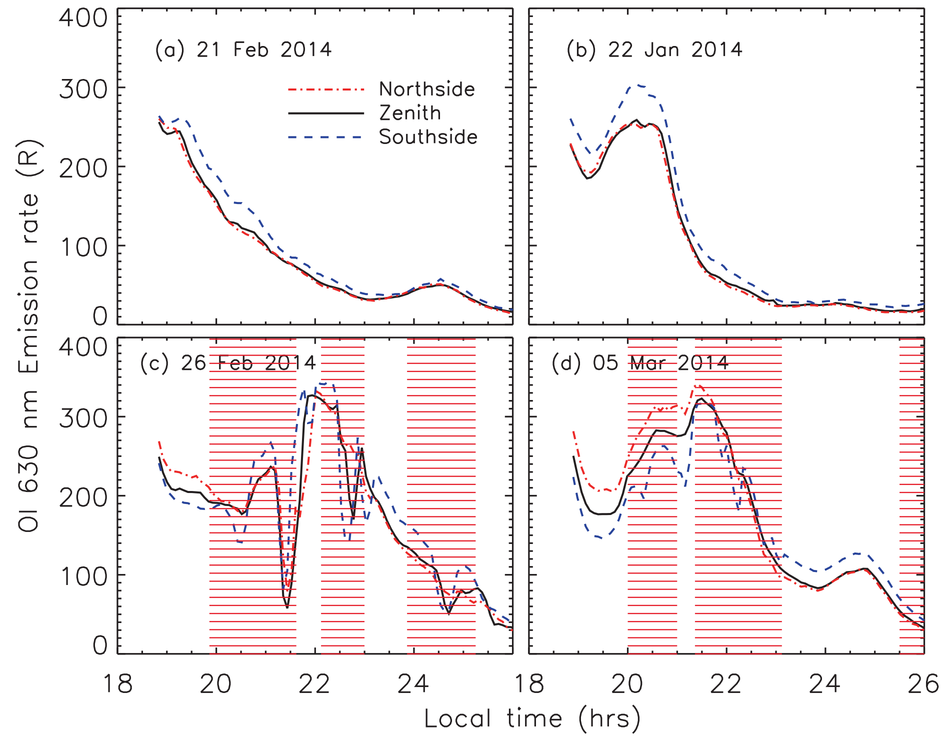

Fig. 1. Typical nightglow variations of OI 630 nm emissions are depicted here. The total FOV of HiTIES is segmented into three sections, one towards North, one South, and Zenith, as indicated in these different colour and line styles. Panel (a) shows monotonic decrease in emissions after the sunset, whereas, panel (b) shows the enhancement in emission during post-sunset time. Panels (c) and (d) show multiple excursions in emissions. The shaded regions in the panels (c) and (d) indicate the time duration of spread-F observed in digisonde, which is situated about 1.5° southward of Mt. Abu.

the OI 630 nm nightglow variations obtained from Mt. Abu are shown. The data gap in the bottom panels is due to non-availability of the data at that time. Interestingly, for four nights, 24 Feb, 26 Feb, 04 Mar, and 05 Mar (Fig. 2a-h), all the depletions in emissions observed over Mt. Abu have a clear correspondence with plasma bubbles seen in all-sky images obtained over Kolhapur in simultaneity, which confirms that the depletion signatures observed over Mt. Abu are due to the plasma bubbles present over latitudes corresponding to that of Mt. Abu. There are several examples of nights when the plasma bubbles did not reach over to Mt. Abu although they had been observed over Kolhapur. For example, on the nights of 24 and 25 Mar (Fig. 2i-l), only one or two bubbles have reached over Mt. Abu, although many more are seen over Kolhapur. It is important to take into cognisance that the distance between the northernmost location presented in the ASI data and the southernmost view direction, as presented in Fig. 2, is around 400 km. Thus, it is understandable that not all plasma bubbles seen in the ASI data from Kolhapur will be present in the HiTIES data over Mt. Abu. Another important aspect that can be noticed is that the depletions in emissions are not equal in all the three different directions (north, zenith, and south) as observed from Mt. Abu, with relatively deeper and also sometimes wider in the emission variability towards south. As the plasma bubbles are aligned along the magnetic field lines and as the different latitudes are mapped to different apex altitudes over the dip equator, it can be inferred that the electron density depletion is greater at lower altitudes over the magnetic equator as compared to those higher above.

Although visually the depletions in both the HiTIES and ASI data seem similar, to make a qualitative assessment, we have carried out spectral analysis of the data, wherein, the emissions obtained from the southernmost direction from HiTIES (around 125 km away from the zenith of Mt. Abu) are compared with the emissions obtained in the northern-most segment of the ASI imager (around 300 km away from the zenith of Kolhapur). The result from the Lomb-Scargle time period analysis (Lomb, 1976; Scargle, 1982) for these two datasets is shown in Fig. 3 for two sample nights with a 90 % confidence level (shown in a horizontal line) out of the nights as shown in Fig. 2. The solid black line indicates the normalized power spectral density (PSD) for different periodicities over southernside of Mt. Abu, whereas, the dashed blue line indicates normalized PSD over northernside of Kolhapur. Fig. 3a shows the presence of periodic fluctuations of less than 1 hr for 24 Feb 2014, whereas, Fig. 3b indicates the periodicities greater than 2 hrs for 04 Mar 2014. The similar periodicities as observed in plasma bubble depletions from the analysis as discussed above and depicted in Fig. 3a and 3b suggest that these are consistently present at both the locations for these and other nights as well (not shown here). As already mentioned above, the physical separation between the locations from these two datasets is around

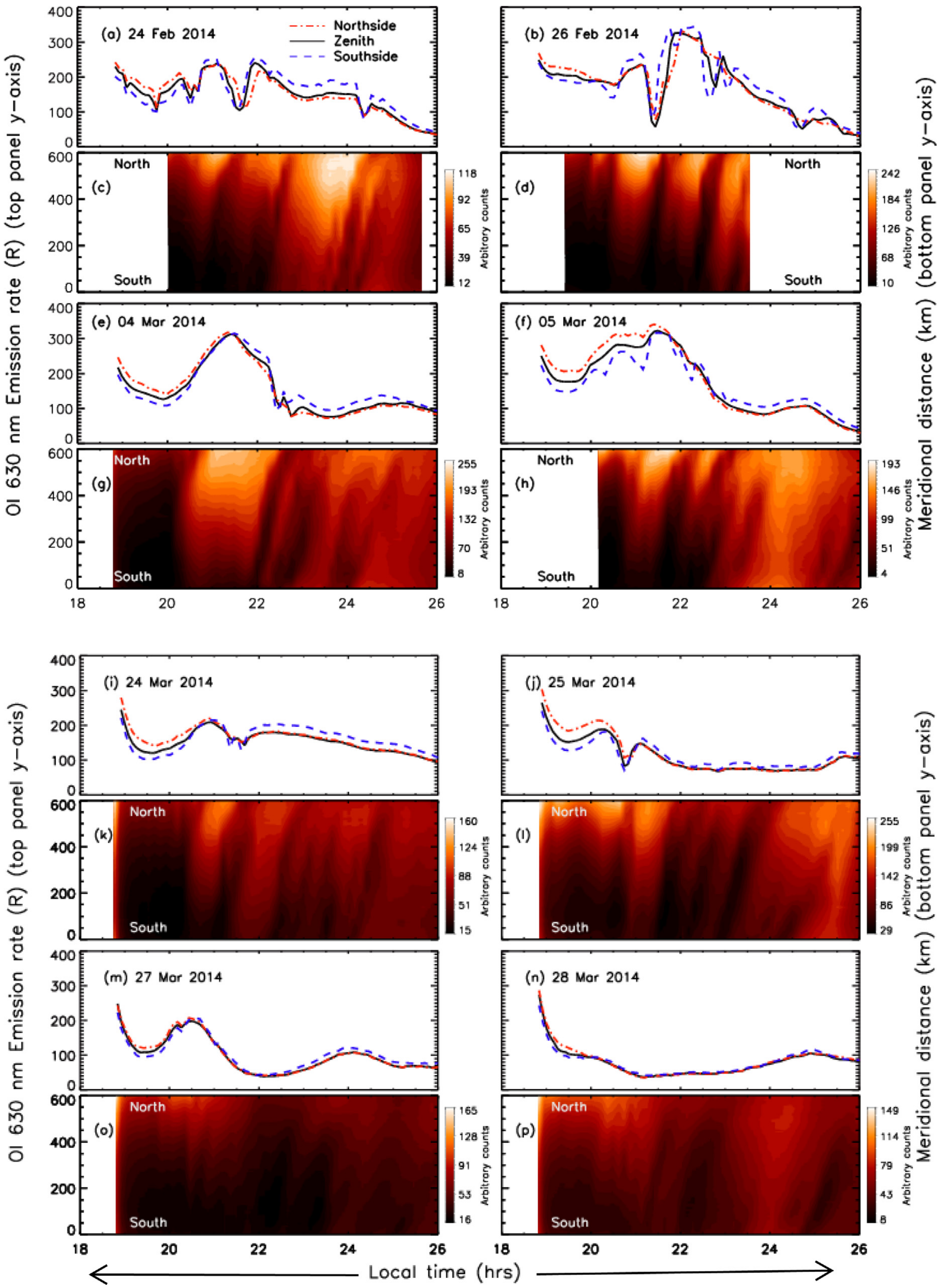

Fig. 2. OI 630 nm emission variations for eight nights as observed over Mt. Abu are shown in top panels a, b, e, f, i, j, m, and n, whereas, the keograms in the bottom panels c, d, g, h, k, l, o, and p show OI 630 nm emission variations in the south-north direction over Kolhapur. The y-axis of the top panels indicates that the OI 630 nm emission rates as observed over Mt. Abu whereas, the y-axis for the bottom panels indicates the south-north distance with Kolhapur as the zenith. Whenever the plasma depletions are observed over Mt. Abu, plasma bubbles are also observed over Kolhapur simultaneously, but the converse is not true.

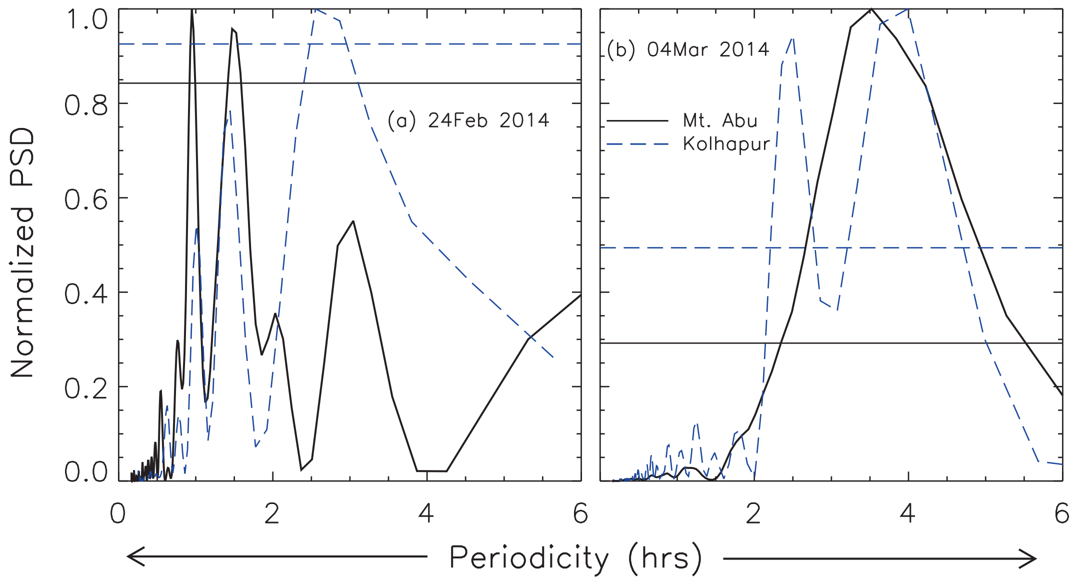

Fig. 3. The Lomb-Scargle periodicities obtained for two sample nights as observed over both the places, Mt. Abu and Kolhapur are presented. Emissions obtained from the Southernmost view direction from Mt. Abu and northern-most as viewed from Kolhapur, which are separated by around 400 km are used in these analyses.

400 km, and therefore, it is expected that not all the periodicities are present with similar strengths at both the locations. A case in point can be seen on 24 Feb 2014 (Fig. 3a), wherein all the periodicities around 1.0, and 1.5 are seen in data at Mt. Abu, while a period of 2.5 hr is present in data at Kolhapur. Nevertheless, the periodicities of 1.0 and 1.5 hr in data at Kolhapur and 2.5 hr in data at Mt. Abu are conspicuous, albeit with lower strength than their respective confidence limits. In Fig. 3b, it can be noted that there are more number of significant periodicities in the data of Kolhapur, which is closer to the magnetic equator and so, it is more likely to record signature of plasma bubbles that extend only closer to the magnetic equator.

The apex altitude to which these bubbles are required to be raised is over 1000 km at the magnetic equator in order for them to reach the latitudes of Mt. Abu. The vertical uplift of the plasma during the sunset time depends upon the strength of the PRE in the zonal electric field during that time (Abadi et al., 2015). The rate of change in the height of the F-layer is used as a proxy for the eastward electric field. An increase in the height of the F-layer happens during sunset time due to an increase in PRE in the electric field. At lower altitudes, due to the recombination of plasma, the ionospheric F-layer shows apparent vertical drift. Bittencourt and Abdu (1981) showed that the effect of recombination is negligible when the F-layer height reaches above 300 km. To minimize the uncertainty in vertical drift measurements that can arise due to recombination at the lower F-region altitudes, we have used the rate of change of the height corresponding to the returned echo of 7 MHz isoelectron density contour to calculate the F-layer vertical drift over Trivandrum. The strength of the PRE has been characterized by taking 30 min average centred at the time of occurrence of peak value in PRE. Out of the 51 nights of available PRE data over Trivandrum, we have found around 21 nights when the optical emissions over Mt. Abu showed sharp depletions due to plasma bubbles. Fig. 4 depicts the variation of PRE strength with the day of year (DOY). The red points indicate the values of the PRE on the nights when the plasma depletions extended until the latitudes of Mt. Abu. On all these nights spread-F had occurred as observed over Trivandrum (except for two; DOY 22 and 52). The red circles indicate the days when EPBs are observed over Kolhapur which are used in this study. It can be seen whenever the plasma

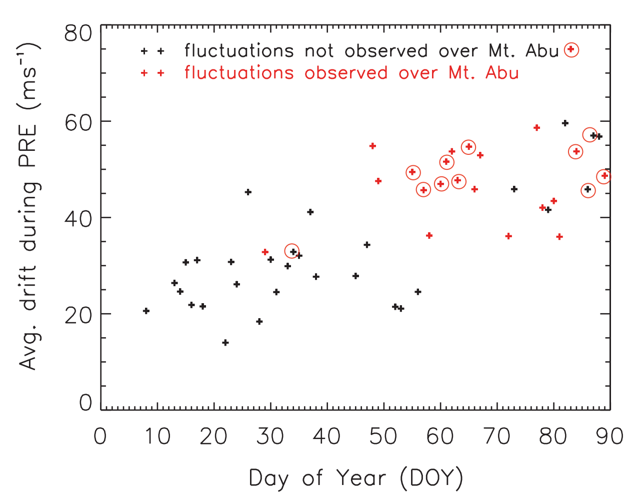

Fig. 4. Avg. PRE strength with day of year (DOY) during Jan-Mar in the year of 2014 is shown. The points in red colour indicate the presence of plasma depletions as observed in the OI 630 nm emission data over Mt. Abu. The EPBs observed in the all-sky imager data used in this study over Kolhapur is indicated in red circles. With the observation of these nights, it can be seen that whenever the depletions are observed over Mt. Abu, the EPBs have been observed over Kolhapur.

depletions are seen over Mt. Abu, the EPBs have been observed over Kolhapur. Due to the high strength of PRE, the plasma bubbles were lifted up to high altitudes (greater than1000 km) which enabled them to reach over Mt. Abu. The plasma depletions over Mt. Abu have been observed on most of the occasions when the PRE values are in the range of 40–60 ms^{-1}. Here, it is emphasised that PRE plays an important role in extending the depletion of electron densities to be mapped over the latitudes along the geomagnetic field lines rather than PRE as the seeding factor (as the discussion corresponds to the developments after the bubble generation). On some occasions, the plasma bubble was absent over Mt. Abu, although large values of PRE were present (for example, DOY: 73, 79, 82, 86, 87, 88). However, plasma bubbles were seen in the ASI data over Kolhapur on the two nights of available data (DOY: 86 & 87) as also shown in Fig. 2o, and 2p (27, 28 Mar). On the night of DOY 87, spread-F was not even observed in the digisonde data at Ahmedabad (although located equatorward of Mt. Abu). We have also looked into the concurrent observation of the C/NOFS satellite data which has an inclination angle of 13° to explore the electron density variation near the equatorial region during these nights when the all-sky imager data were unavailable. As per the availability of C/NOFS data, the electron densities are shown to exhibit sharp decreases on all nights (not shown here) not only when the depletions were observed over Mt. Abu, but also when the depletions were not observed over Mt. Abu on the days mentioned above (DOY: 73, 86, 87, 88). Several factors, such as, elec-

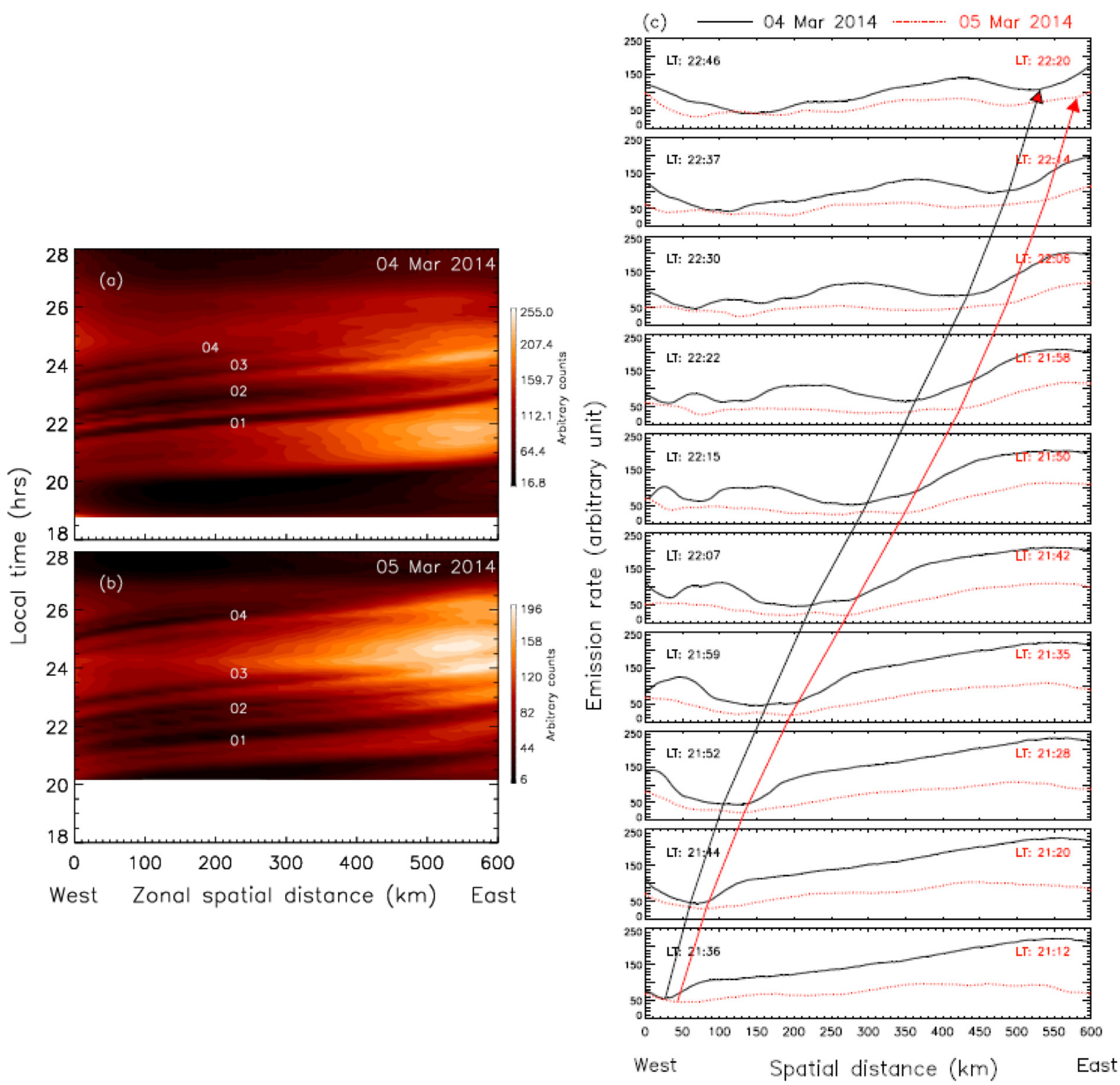

Fig. 5. Zonal variations in OI 630 nm emissions have been depicted with time for two neighbouring nights in panels (a) and (b). A zonal strip for each image (12 km centred over zenith × 600 km) is considered. The zonal movement of the plasma bubble marked as ‘01′ for the nights 04 Mar and 05 Mar 2014 has been shown over the time in panel (c).

tric fields, and neutral winds, could have prevented the plasma bubbles from reaching to Mt. Abu later in the night in spite of large magnitudes of PRE earlier on those nights. This will be taken up in different study.

We have calculated the zonal drift speeds in the plasma depletions using the nightly images as the bubbles move zonally with time. The zonal (12 km over zenith × 600 km along west-east) segment in each image is considered and they are stacked one above the other as shown in Fig. 5. By observing the spatial movement with time of depletions in emissions caused due to the plasma bubbles, we have calculated their zonal drift speeds. As can be seen from Fig. 5a and 5b for 04 and 05 Mar 2014, different bubbles keep appearing as time progresses (as shown in the y-axis), beginning from the westernmost location of the FOV, moving eastwards, and disappearing. The times corresponding to the bubbles' appearance and disappearance are noted along with the spatial distances to calculate the average zonal drift speeds of each plasma bubble. Four plasma bubbles have been marked on these nights in the figure. It can be seen that the bubble 01 is seen to be present over the whole 600 km in the west-east direction for a long duration on both nights, whereas, the other bubbles do not last that long. Further, the first bubble is the deepest and widest of all. Such behaviour in the zonal extent has been seen on the other nights also (not shown here). There is another bubble that can be seen on 05 Mar around 20 LT (before the one marked by 01), and as this was present even before the first image was obtained on that night, it is not used for the estimation of the drift speed. The spatial movements of the plasma bubble 01 for the night 04 Mar and 05 Mar 2014 as seen over zonal strip centered over zenith are depicted in solid black and dotted red lines, respectively (Fig. 5c). The time evolution of each frame of the Fig. 5c is mentioned on the left and right sides for the nights of 04 Mar and 05 Mar 2014, respectively. From the time evolution of the depletions seen in the frames as shown in Fig. 5c, it can be seen that they have travelled around 510 km and 540 km with zonal speeds of around 121.4 and 132.4 ms^{-1} for 04 Mar and 05 Mar 2014, respectively. Similarly, the zonal drift values for the other plasma bubbles for different nights have also been calculated and are shown in Fig. 6.

Fig. 6 shows the zonal drift values of the plasma bubbles for a total 14 nights which include those plasma bubbles that have crossed the zenith location. It can be seen that the zonal speeds are higher during the post-sunset time, and they decrease as the night progresses. The orange line in the Fig. 6 shows the temporal variation of average zonal drift where all the values in a given 30 min duration are averaged. In an earlier study over Brazilian sector, the zonal speeds were shown to be different at different sides of plasma bubble structures, like, western wall, central depletion and eastern wall (Pimenta et al., 2001). It was reported in that work that the eastern wall showed an increase in speed of around 40 % as compared with the western wall, whereas, the central depletion showed an increase by 10–20 %. The present investigations over Indian longitudes reported here did not reveal such differential variations in speeds for different sides of plasma walls. The current result of the plasma bubble drift speed matches well with the earlier reports over Indian sector (Mukherjee et al., 2003, Gurav et al., 2018; Ghodpage et al., 2021). The background plasma and the plasma bubble zonal drift showed good correlation with the measured eastward neutral winds (Chapagain et al., 2012, 2013). The similarity in the variation in the zonal drifts of the EPBs and the zonal wind speeds had been interpreted to be due to the internal space–time dynamics of the EPBs as the perturbed electric field generated inside the EPBs can affect the drift motion.

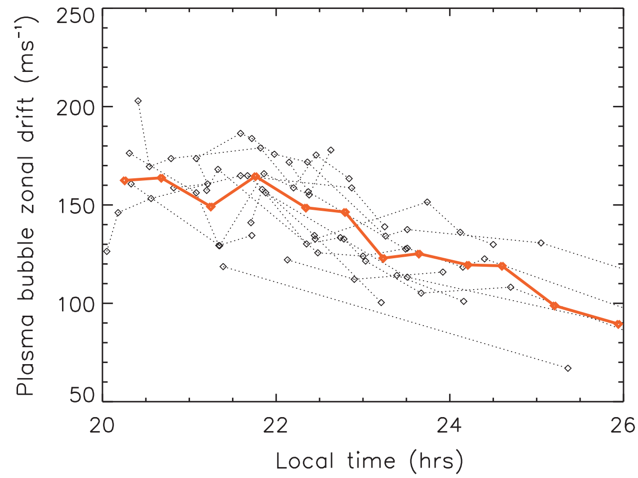

Fig. 6. Zonal drift speeds of the plasma bubbles are depicted for 14 nights. The orange line shows the 30-minutes average values.

4. Discussion

In the previous section, we have discussed about the plasma depletions observed over two low-latitudinal regions, Mt. Abu and Kolhapur. As discussed, the 100° FOV of the all-sky imager data provides spatial coverage with a range of 300 km radius centred over Kolhapur. We have carried out the wave number spectral analysis from the OI 630 nm images using the Lomb-Scargle periodogram analysis by taking 600 km west-east strip over the zenith for each image of a given night. This analysis yields the information of zonal scales of that particular time. In Fig. 7, we depict the contour plot using the information of zonal scale sizes that are obtained by such spectral analysis at different times on a given night. A contrasting behaviour of zonal scale size has been noticed between the nights when the plasma bubbles are present (03 Feb and 24 Feb 2014) and when they are absent (04 Feb and 25 Feb 2014). Fig. 7a, b and 7c, d show the data from two neighbouring nights which clearly depicts a clear contrast between these nights. The 99 % confidence level for various frequencies has been estimated, and it is 0.2 or smaller in terms of the normalized PSD. It can also be

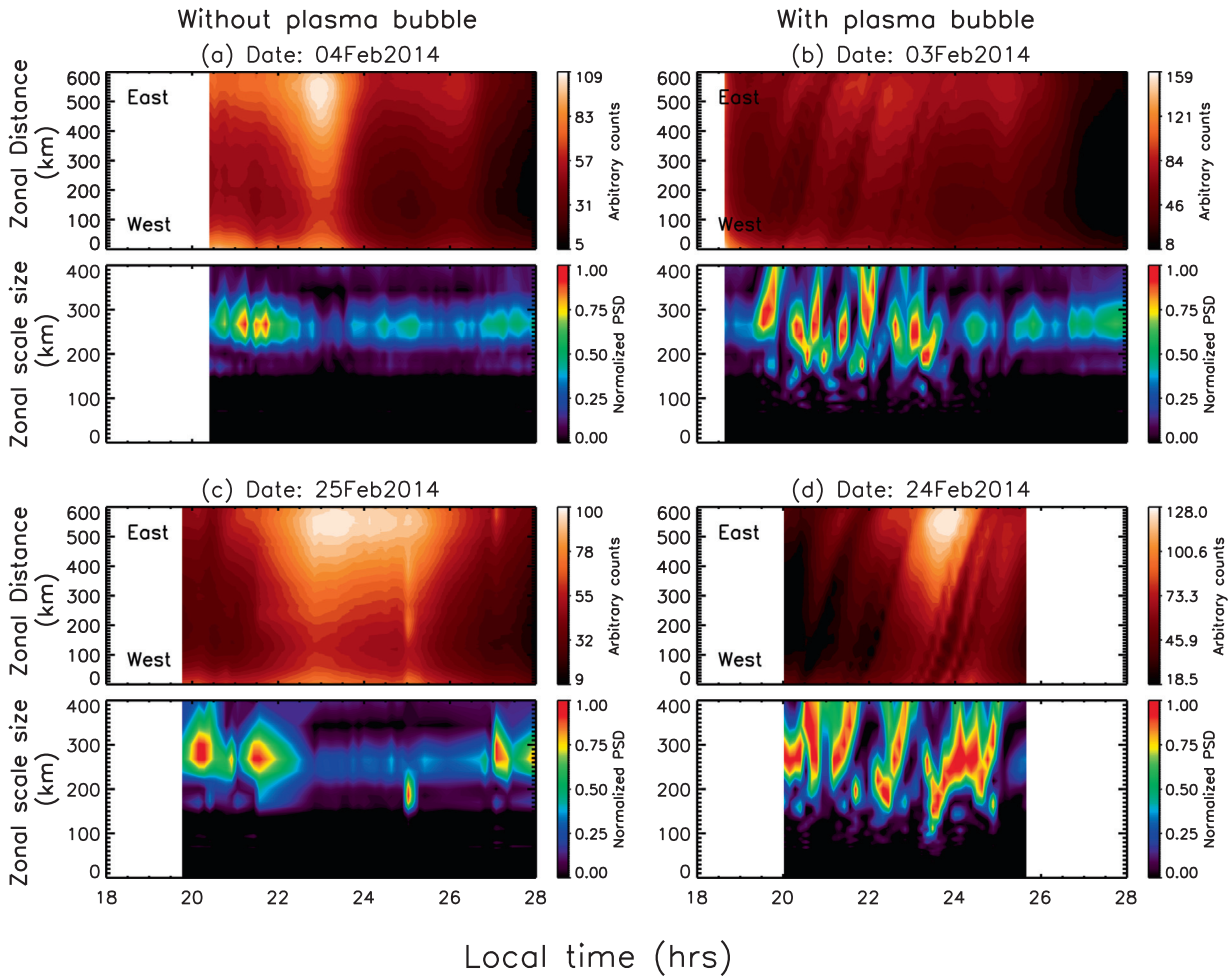

Fig. 7. The zonal spatial variation and scale sizes are shown in OI 630 nm emissions as observed over Kolhapur for four different nights. The values of scale sizes show contrasting behaviour between the nights with the occurrence of EPBs and those with the absence of the EPBs.

noted that for all the nights the scale sizes in the range of 250–300 km are present with larger power in comparison to those of 150–200 km range. On the nights that showed the presence of EPBs, several smaller scale sizes were noticed (Fig. 7b, d) which is in stark contrast with the nights that did not show any presence of EPBs (Fig. 7a, c).

Different scale sizes are significant (as seen in the PSD values) at different times. Therefore, the percentage occurrence and the averaged PSD value of a given range of scale size are obtained for a given night. The estimated scale sizes have been binned in 50 km grids as shown in Fig. 8a-d with the number of occurrences for a given range of scale size, whereas, the Fig. 8e-h shows the average PSD value for that particular range of scale size. Suppose for different scale size bins, λ_i (i = 1, 2, 3, 4, ...), the number of occurrences is found to be n_i, the percentage of occurrences in a given scale size bin has been calculated as, $(n_i/\Sigma n_i) \times 100$ %. Now, for a given scale size bin, λ_i, if the number of occurrences of that bin is n_i and normalized PSD values of each occurrence are p_k (k = 1, 2, ..., n_i), then the average PSD value has been calculated as, $\Sigma p_k/n_i$ for that given scale size bin. The data corresponding to the nights as shown in Fig. 7 are depicted in Fig. 8. Scale sizes above the 99 % confidence level have been considered in this representation. A clear contrast is seen in terms of the percentage occurrences of different scale sizes between the nights with and without the presence of EPBs. The dominant 150–200 km and 250–300 km zonal scale sizes on the nights without EPBs (Fig. 8a, c) are interpreted to be the typical scale sizes of the GWs present in the ionosphere-thermosphere region, as these are also present on the nights with the EPB occurrences (Fig. 8b, d). However, the shorter scale sizes can be seen on the nights with the EPB occurrence only (Fig. 8b, d). Moreover, not only does the percentage occurrence of shorter scale sizes, but also their average PSD values show an increase during the nights with the occurrence of EPBs (Fig. 8f, h). This clearly shows the significance of shorter scales during the nights with EPB occurrence. This type of contrast in scale sizes is seen for the other nights as well. Thus, the plasma bubble characteristics associated with it, like the inter-bubble separation(s), bifurcation of bubbles, widths of the bubble, etc., change with time. The contrast in scale sizes as observed between EPB and non-EPB nights provides important information on the state of nighttime ionosphere thermosphere regions during the presence of plasma bubbles. Such characterization in the zonal GW

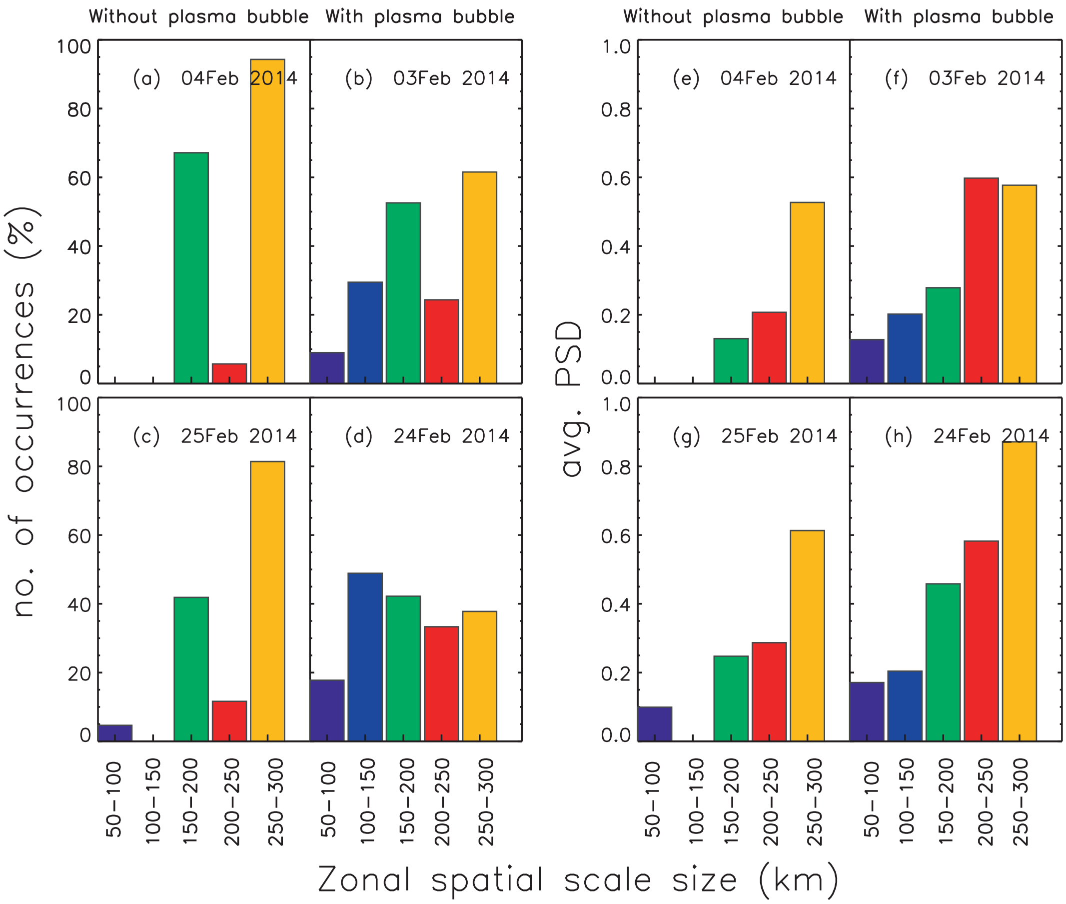

Fig. 8. The scale sizes are put in 50 km grid which are shown in x-axis. The percentage occurrence of a given scale size and the average PSD values of the corresponding scale sizes are shown in the y-axis of the left and right-side figures, respectively.

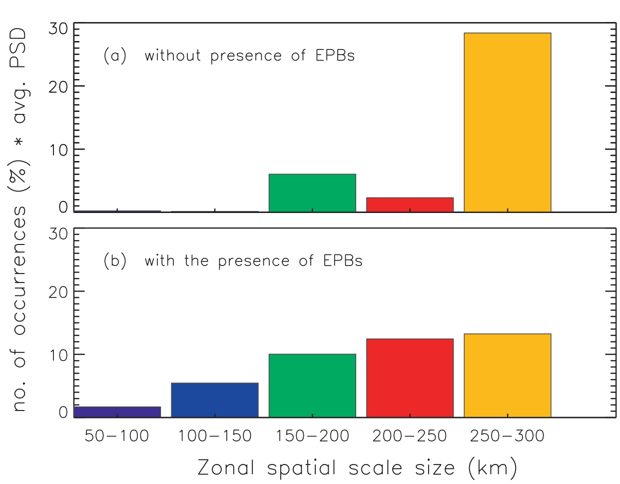

Fig. 9. The scale sizes which are segregated in 50 km grids are compared between the cases when the bubbles appeared in the image and when they did not. In the y-axis the collective effect of number of occurrence and PSD value for a given scale size has been shown by calculating the product of these two. The top panel includes all the images when the bubbles were not observed and the bottom panel shows the distribution of scale sizes when the plasma bubbles were observed in the images.

behaviour using the information of multiple number of nights has not been presented in the literature so far, to the best of our knowledge.

The GWs are one of the potential factors in the seeding of the plasma bubbles that triggers the Rayleigh-Taylor instability (e.g., Kelley et al., 1981; Huang and Kelley, 1996; Makela et al., 2010). The 250–300 km scale sizes have been found to be omnipresent irrespective of the presence/absence of plasma bubbles indicating that this is a neutral GW scale size typically existing at all times in the upper atmosphere. Further, smaller length scales are found to be present during the nights when EPBs were observed. The GWs with smaller scale sizes seem to be playing an effective role in the generation of plasma bubbles. These scale sizes on the nights with EPB occurrence also coincide with the inter-bubble distance. From the literature reported earlier, the inter-bubble spacings had been shown to have a good correlation with the horizontal GW wavelengths (Takahashi et al., 2009; Makela et al., 2010; Das et al., 2020). The inter-bubble spacing measured from radar data over Gadanki in Indian longitudes, has been shown to be following a linear relationship with the horizontal wavelengths of GWs as estimated from the collocated data from ionosonde (Das et al., 2020). In an earlier report, Makela et al. (2010) categorized the plasma bubble spacings as seen over Chile, low-latitude location in the southern hemisphere, using three years of optical data. With the support of ray tracing method as discussed by Vadas and Crowley

(2010), these bubble spacings were considered as evidence of horizontal wavelength of GWs, which are mostly secondary GWs present at this thermospheric altitudes. The presence of the small-scale wave-like structure (SSWS) as seen in the inter-bubble depletion is discussed in some earlier reports with some numerical simulation (Sekar et al., 2001) and a case study (Narayanan et al., 2012). Our result experimentally establishes the presence of such smaller-scale wave structures using the observation of around 14 nights during the period Feb-Mar in the year of 2014 when the EPBs were observed. It is proposed that these smaller scale size GWs in the zonal direction in the range of 50–150 km are potential seeds that triggered the occurrence of plasma bubbles.

To buttress the proposition further, we have considered both the factors, number of occurrence of a given range of scale size and the normalized strength on each occasion, as depicted in Fig. 8 and have shown the result in Fig. 9. Fig. 9 shows distribution of scale sizes between the two categories of presence of EPBs and absence of EPBs. Here, we have first calculated the scale sizes for each of the images that are present at 7–8 min cadance and obtained a product of the average PSD value of a given scale size and the percentage of occurrence of that scale size for a given night. This takes into account, both, their strength and number of occurrences of a given scale size. Around 1290 images have been analysed for 20 nights among which 688 images showed the presence of plasma bubble signatures, which is around 53 %. Therefore, this analysis can be considered to yield a fair comparison between the behaviour of the zonal GW characteristics in both the categories of existence and absence of EPBs. It is evident from Fig. 9 that there is strong occurrence of 250–300 km scale size in non-EPB images (similar to that seen in 04, 25 Feb 2014 in Fig. 8), whereas, when the EPBs are present, the power corresponding to zonal scale sizes shorter than 250 km is also seen to be increasing. The power in the 250–300 km scale sizes seems to be redistributed among the shorter scale sizes like 200–250 km, 150–200 km, 100–150 km. As also stated above, these scale sizes give a fair indication of the inter-bubble spacings. The crests of the GW in the zonal direction are likely to give rise to the density depletion as the low-density plasma from lower altitudes is lifted upwards over the equator, which is mapped as a bubble along a given longitude as seen in optical all-sky images over Kolhapur. In this comprehensive study, we have shown experimental evidence of the presence of GW scale size less than 250 km, possibly serving as the seed perturbation of EPBs for a given night.

5. Summary

OI 630 nm nighttime airglow emissions have been investigated over Mt. Abu, a low-latitude location. Multiple excursions have been found in the OI 630 nm emissions on some nights. Simultaneous radio observations using ionosonde from a nearby location, Ahmedabad, exhibited spread in the reflected echoes exactly at the times when depletions were observed in the nightglow emissions. We have also analysed the OI 630 nm emissions obtained using an all-sky imager from Kolhapur, which is situated between the low-latitude and the dip equatorial locations. Whenever depletions in the OI 630 nm nightglow are seen at Mt. Abu, plasma bubbles are seen in simultaneity over Kolhapur. The strength of the PRE was found to be larger on the nights when the depletions in emissions were observed in the OI 630 nm emission over Mt. Abu, indicating that the bubbles rose over 1000 km at the magnetic equator on those occasions. The plasma bubbles generated due to Rayleigh-Taylor instability over the magnetic equator move eastwards as the night progresses along with the zonal wind. The zonal speeds of the plasma bubbles estimated from all-sky imager data over Kolhapur have been found to be varying in the range around 190–90 ms^{-1}, decreasing in magnitudes from post-sunset to midnight. Further, we have also carried out wave number analyses for the emissions in the zonal direction for around 1300 images with nearly equal number with occurrence and absence of EPBs. It is found that, typically, during nighttime the zonal scale sizes are in the range of 150–200 km and 250–300 km (with a greater strength in the latter scale-size) on geomagnetic quiet nights without the presence of any plasma bubbles. The zonal scale sizes show contrasting behaviour between the nights with the EPB and without the occurrence of EPBs. The scale sizes of GWs smaller than 250 km have been observed on almost all the times whenever the plasma bubbles were present, which correspond to the inter-bubble separation distance. As the bubble depletions over the magnetic equator most likely occur at the crest location of the GW, the zonal distances between the bubbles, as seen in a location close to the magnetic equator can be assumed to represent the zonal scale sizes of GWs over the equator. Therefore, it is proposed that the GW scale sizes in the zonal direction of smaller than 250 km, if present, in the evening could potentially act as the triggers for the generation of plasma bubbles.

Declaration of Competing Interest

The authors declare that they have no known competing financial interests or personal relationships that could have appeared to influence the work reported in this paper.

Acknowledgement

The nighttime spectrograph data used in this study have been obtained from PRL's optical aeronomy observatory at Gurushikhar which is maintained by the Physical Research Laboratory. All-sky imager data are obtained from Indian Institute for Geomagnetism, Shivaji University campus, Kolhapur, India. The digisonde data of the locations at AMD and TVM are obtained from the Physical Research Laboratory, Ahmedabad and Space Physics Laboratory, Trivandrum, respectively. The C/NOFS data have been obtained from https://cdaweb.gsfc.nasa.gov/index.html. SS acknowledges the discussions carried out with Sunil Kumar, Subir Mandal, and Dupinder Singh during this work. This work is supported by the Department of Space, Government of India.

References

Abadi, P., Otsuka, Y., Tsugawa, T., 2015. Effects of pre-reversal enhancement of E × B drift on the latitudinal extension of plasma bubble in Southeast Asia. Earth Planet and Space 67–74. https://doi.org/10.1186/s40623-015-0246-7.

Abdu, M.A., Batista, I.S., Kantor, I.J., Sobral, J.H.A., 1982. Gravity wave induced ionization layers in the night F-region over Cachoeira Paulista (22°S, 45°W). J. Atmos. Terr. Phys. 44 (9), 759–767. https://doi.org/10.1016/0021-9169(82)90004-6.

Abdu, M.A., De Medeiros, R.T., Bittencourt, J.A., Batista, I.S., 1983. Vertical ionization drift velocities and range type spread F in the evening equatorial ionosphere. J. Geophys. Res. Space Phys. 88 (A1), 399–402. https://doi.org/10.1029/JA088iA01p00399.

Abdu, M.A., Alam Kherani, E., Batista, I.S., De Paula, E.R., Fritts, D.C., Sobral, J.H.A., 2009. Gravity wave initiation of equatorial spread F/plasma bubble irregularities based on observational data from the SpreadFEx campaign. Ann. Geophys. 27 (7), 2607–2622. https://doi.org/10.5194/angeo-27-2607-2009.

Balsley, B.B., Haerendel, G., Greenwald, R.A., 1972. Equatorial spread F: recent observations and a new interpretation. J. Geophys. Res. 77 (28), 5625–5628. https://doi.org/10.1029/JA077i028p05625.

Bittencourt, J.A., Abdu, M.A., 1981. Theoretical comparison between apparent and real vertical ionization drift velocities in the equatorial F region. J. Geophys. Res. 86, 2451–2454. https://doi.org/10.1029/JA086iA04p02451.

Chakrabarti, S., Pallamraju, D., Baumgardner, J., Vaillancourt, J., 2001. HiTIES: a high throughput imaging echelle spectrograph for ground-based visible airglow and auroral studies. J. Geophys. Res. 106 (A12), 30337–30348. https://doi.org/10.1029/2001JA001105.

Chapagain, N.P., Makela, J.J., Meriwether, J.W., Fisher, D.J., Buriti, R. A., Medeiros, A.F., 2012. Comparison of nighttime zonal neutral winds and equatorial plasma bubble drift velocities over Brazil. J. Geophys. Res.: Space Phy. 117 (A6). https://doi.org/10.1029/2012JA017620.

Chapagain, N.P., Fisher, D.J., Meriwether, J.W., Chau, J.L., Makela, J.J., 2013. Comparison of zonal neutral winds with equatorial plasma bubble and plasma drift velocities. J. Geophys. Res. Space Phys. 118 (4), 1802–1812. https://doi.org/10.1002/jgra.50238.

Farley, D.T., Balsey, B.B., Woodman, R.F., McClure, J.P., 1970. Equatorial spread F: implications of VHF radar observations. J. Geophys. Res. 75 (34), 7199–7216. https://doi.org/10.1029/JA075i034p07199.

Ghodpage, R.N., Taori, A., Patil, P.T., Gurubaran, S., Sripathi, S., Banola, S., Sharma, A.K., 2014. Simultaneous optical measurements of equatorial plasma bubble (EPB) from Kolhapur (16.8°N, 74.2°E) and Gadanki (13.5°N, 79.2°E). J. Atmos. Terr. Phys. 121, 196–205. https://doi.org/10.1016/j.jastp.2014.05.008.

Ghodpage, R. N., Gurav, O. B., Taori, A., Sau, S., Patil, P. T., Erram, V. C., & Sripathi, S., 2021. Observation of an intriguing equatorial plasma bubble event over Indian sector. Journal of Geophysical Research: Space Physics, 126(5), e2020JA028308. https://doi.org/10.1029/2020JA028308.

Das, S.K., Patra, A.K., Kherani, E.A., Chaitanya, P.P., Niranjan, K., 2020. Relationship between presunset wave structures and interbubble spacing: the seeding perspective of equatorial plasma bubble. Journal of Geophysical Research: Space Physics, 125(8), 2020JA028122. https://doi.org/10.1029/2020JA028122.

Gurav, O.B., Sharma, A.K., Ghodpage, R.N., Nade, D.P., Chavan, G.A., Gaikwad, H.P., Patil, P.T., 2018. Zonal drift velocity of equatorial plasma bubbles during ascending phase of 24th solar cycle using all sky imager over Kolhapur, India. J. Geophys. Res. Sp. Phys. https://doi.org/10.1029/2018JA025810.

Gurav, O.B., Narayanan, V.L., Sharma, A.K., Ghodpage, R.N., Gaikwad, H.P., Patil, P.T., 2019. Airglow imaging observations of some evolutionary aspects of equatorial plasma bubbles from Indian sector. Adv. Space Res. 64, 385–399. https://doi.org/10.1016/j.asr.2019.04.008.

Haerendel, G., Eccles, J.V., Cakir, S., 1992. Theory for modeling the equatorial evening ionosphere and the origin of the shear in the horizontal plasma flow. J. Geophys. Res. Space Phys. 97 (A2), 1209–1223. https://doi.org/10.1029/91JA02226.

Huang, C.S., de La Beaujardiere, O., Roddy, P.A., Hunton, D.E., Ballenthin, J.O., Hairston, M.R., 2013. Long-lasting daytime equatorial plasma bubbles observed by the C/NOFS satellite. J. Geophys. Res. Space Phys. 118 (5), 2398–2408. https://doi.org/10.1002/jgra.50252.

Huang, C.S., Kelley, M.C., 1996. Non-linear evolution of equatorial spread F: 2. Gravity wave seeding of Rayleigh-Taylor instability. J. Geophys. Res.: Space Phys. 101 (A1), 293–302. https://doi.org/10.1029/95JA02210.

Huang, C.S., Roddy, P.A., 2016. Effects of solar and geomagnetic activities on the zonal drift of equatorial plasma bubbles. J. Geophys. Res. Space Phys. 121 (1), 628–637. https://doi.org/10.1002/2015JA021900.

Huba, J.D., Joyce, G., Krall, J., 2008. Three-dimensional equatorial spread F modeling. Geophys. Res. Lett. 35, L10102. https://doi.org/10.1029/2008GL033509.

Karan, D.K., Daniell, R.E., England, S.L., Martinis, C.R., Eastes, R.W., Burns, A.G., McClintock, W.E., 2020. First zonal drift velocity measurement of Equatorial Plasma Bubbles (EPBs) from a geostationary orbit using GOLD data. Journal of Geophysical Research: Space Physics, 125(9),2020JA028173. https://doi.org/10.1029/2020JA028173.

Kelley, M.C., 1985. Equatorial spread F: Recent results and outstanding problems. J. Atmos. Terr. Phys. 47 (8–10), 745–752. https://doi.org/10.1016/00219169(85)90051-0.

Kelley, M.C., Hysell, D.L., 1991. Equatorial spread-F and neutral atmospheric turbulence. a review and a comparative anatomy. J. Atmos. Sol. Terr. Phys. 53, 695–708. https://doi.org/10.1016/0021-9169(91)90122-N.

Kelley, M.C., Larsen, M.F., LaHoz, C., McClure, J.P., 1981. Gravity wave initiation of equatorial spread F: a case study. J. Geophys. Res. 86, 9087. https://doi.org/10.1029/JA086iA11p09087.

Kelley, M.C., Makela, J.J., Ledvina, B.M., Kintner, P.M., 2002. Observations of equatorial spread-F from Haleakala, Hawaii. Geophys. Res. Lett. 29 (20). https://doi.org/10.1029/2002GL015509.

Kil, H., Paxton, L.J., Oh, S.J., 2009. Global bubble distribution seen from ROCSAT-1 and its association with the evening prereversal enhancement. J. Geophys. Res. Space Phys. 114. https://doi.org/10.1029/2008JA013672 A06307.

Krall, J., Huba, J.D., Martinis, C.R., 2009. Three-dimensional modeling of equatorial spread F airglow enhancements. Geophys. Res. Lett. 36 (10). https://doi.org/10.1029/2009GL038441.

Lomb, N.R., 1976. Least-squares frequency analysis of unequally spaced data. Astrophys. Space Sci. 39 (2), 447–462. https://doi.org/10.1007/BF00648343.

Makela, J.J., Kelley, M.C., 2003. Field-aligned 777.4-nm composite airglow images of equatorial plasma depletions. Geophys. Res. Lett. 30 (8). https://doi.org/10.1029/2003GL017106.

Makela, J.J., Vadas, S.L., Muryanto, R., Duly, T., Crowley, G., 2010. Periodic spacing between consecutive equatorial plasma bubbles. Geophys. Res. Lett. 37 (14). https://doi.org/10.1029/2010GL043968.

Maruyama, T., Matuura, N., 1984. Longitudinal variability of annual changes in activity of equatorial spread F and plasma bubbles. J. Geophys. Res. Space Phys. 89 (A12), 10903–10912. https://doi.org/10.1029/JA089iA12p10903.

Mendillo, M., Baumgardner, J., 1982. Airglow characteristics of equatorial plasma depletions. J. Geophys. Res. Space Phys. 87 (A9), 7641–7652. https://doi.org/10.1029/JA087iA09p07641.

Mendillo, M., Tyler, A., 1983. Geometry of depleted plasma regions in the equatorial ionosphere. J. Geophys. Res. 88 (A7), 5778–5782. https://doi.org/10.1029/JA088iA07p05778.

Mukherjee, G.K., 2003. Studies of equatorial F-region depletions and dynamics using multiple wavelength nightglow imaging. J. Atmos. Sol. Terr. Phys. 65 (3), 379–390. https://doi.org/10.1016/S1364-6826(02)00214-6.

Narayanan, V.L., Taori, A., Patra, A.K., Emperumal, K., Gurubaran, S., 2012. On the importance of wave-like structures in the occurrence of equatorial plasma bubbles: a case study. J. Geophys. Res. 117, A01306. https://doi.org/10.1029/2011JA017054.

Ossakow, S.L., 1981. Spread-F theories—a review. J. Atmos. Terr. Phys. 43 (5–6), 437–452. https://doi.org/10.1016/0021-9169(81)90107-0.

Otsuka, Y., Shiokawa, K., Ogawa, T., Wilkinson, P., 2002. Geomagnetic conjugate observations of equatorial airglow depletions. Geophys. Res. Lett. 29, 1753. https://doi.org/10.1029/2002GL015347.

Pallamraju, D., Chakrabarti, S., Valladares, C.E., 2004. Magnetic storm-induced enhancement in neutral composition at low latitudes as inferred by O(1D) dayglow measurements from Chile. Ann. Geophys. 22, 3241–3250. https://doi.org/10.5194/angeo-22-3241-2004.

Park, J., Huang, C.-S., Eastes, R.W., Coster, A.J., 2022. Temporal evolution of low-latitude plasma blobs identified from multiple measurements: ICON, GOLD, and Madrigal TEC. Journal of Geophysical Research: Space Physics, 127, e2021JA029992. https://doi.org/10.1029/2021JA029992.

Patra, A.K., Srinivasulu, P., Chaitanya, P.P., Rao, M.D., Jayaraman, A., 2014. First results on low-latitude E and F region irregularities obtained using the Gadanki Ionospheric Radar Interferometer. J. Geophys. Res. Space Phys. 119, 10276–10293. https://doi.org/10.1002/2014JA020604.

Pimenta, A.A., Fagundes, P.R., Bittencourt, J.A., Sahai, Y., Gobbi, D., Medeiros, A.F., Taylor, M.J., 2001. Ionospheric plasma bubble zonal drift: a methodology using OI 630 nm all-sky Imaging systems. Adv. Space Res. 27 (2001), 1219–1224. https://doi.org/10.1016/S0273-1177(01)00201-0.

Prakash, S., Pallamraju, D., Sinha, H.S.S., 2009. Role of the equatorial ionization anomaly in the development of the evening prereversal enhancement of the equatorial zonal electric field. J. Geophys. Res. 114, A02301. https://doi.org/10.1029/2007JA012808.

Raghavarao, R., Gupta, S.P., Sekar, R., Narayanan, R., Desai, J.N., Sridharan, R., Babu, V.V., Sudhakar, V., 1987. In situ measurements of winds, electric fields and electron densities at the onset of equatorial spread-F. J. Atmos. Terr. Phys. 49 (5), 485–492. https://doi.org/10.1016/0021-9169(87)90042-0.

Raghavarao, R., Nageswararao, M., Sastri, J.H., Vyas, G.D., Sriramarao, M., 1988. Role of equatorial ionization anomaly in the initiation of equatorial spread F. J. Geophys. Res. 93 (A6), 5959–5964. https://doi.org/10.1029/JA093iA06p05959.

Raghavarao, R., Hoegy, W.R., Spencer, N.W., Wharton, L.E., 1993. Neutral temperature anomaly in the equatorial thermosphere-a source of vertical winds. Geophys. Res. Lett. 20 (11), 1023–1026. https://doi.org/10.1029/93GL01253.

Rajesh, P.K., Liu, J.Y., Sinha, H.S.S., Banerjee, S.B., 2010. Appearance and extension of airglow depletions. J. Geophys. Res.: Space Phys. 115 (A8). https://doi.org/10.1029/2009JA014952.

Saha, S., Pallamraju, D., Pant, T.K. and Chakrabarti, S., 2021. On the Cause of the Post-Sunset Nocturnal OI 630 nm Airglow Enhancement Over Low-Latitude Thermosphere. Journal of Geophysical Research: Space Physics, 126(7), 2021JA029146. https://doi.org/10.1029/2021JA029146.

Scargle, J.D., 1982. Studies in astronomical time series analysis. II. statistical aspects of spectral analysis of unevenly spaced data. Astron. J. 263 (2), 835–853. https://doi.org/10.1086/160554.

Sekar, R., Kherani, E.A., Rao, P.B., Patra, A.K., 2001. Interaction of two long-wavelength modes in the non-linear numerical simulation model of equatorial spread F. J. Geophys. Res. Space Phys. 106 (A11), 24765–24775. https://doi.org/10.1029/2000JA000361.

Sekar, R., Chakrabarty, D., Pallamraju, D., 2012. Optical signature of shear in the zonal plasma flow along with a tilted structure associated with equatorial spread F during a space weather event. J. Atmos. Sol. Terr. Phys. 75–76, 57–63. https://doi.org/10.1016/j.jastp.2011.05.009.

Sekar, R., Raghavarao, R., 1987. Role of vertical winds on the Rayleigh-Taylor mode instabilities of the nighttime equatorial ionosphere. J. Atmos. Terr. Phys. 49 (10), 981–985. https://doi.org/10.1016/0021-9169(87)90104-8.

Sekar, R., Suhasini, R., Raghavarao, R., 1994. Effects of vertical winds and electric fields in the non-linear evolution of equatorial spread F. J. Geophys. Res. Space Phys. 99 (A2), 2205–2213. https://doi.org/10.1029/93JA01849.

Sharma, A.K., Nade, D.P., Nikte, S.S., Ghodpage, R.N., Patil, P.T., Rokade, M.V., et al., 2014. Development of fast image analysis technique for all-sky images. Curr. Sci., 1–9

Shiokawa, K., Otsuka, Y., Ogawa, T., Wilkinson, P., 2004. Time evolution of high-altitude plasma bubbles imaged at geomagnetic conjugate points. Ann. Geophys. 22, 3137–3143. https://doi.org/10.5194/angeo-22-3137-2004.

Sivakandan, M., Paulino, I., Ramkumar, T.K., Taori, A., Patra, A.K., Sripathi, S., Niranjan, K., Bilibio, A.V., 2019. Multi-instrument investigation of troposphere-ionosphere coupling and the role of gravity waves in the formation of equatorial plasma bubble. J. Atmos. Sol. Terr. Phys. 189, 65–79. https://doi.org/10.1016/j.jastp.2019.04.006.

Sridharan, R., Pallamraju, D., Raghavarao, R., Ramarao, P.V.S., 1994. Precursor to equatorial spread-F in OI 630.0 nm dayglow. Geophys. Res. Lett. 21, 2797–2800. https://doi.org/10.1029/94GL02732.

Sultan, P.J., 1996. Linear theory and modeling of the Rayleigh-Taylor instability leading to the occurrence of equatorial spread F. J. Geophys. Res. 101 (A12), 26875–26891. https://doi.org/10.1029/96JA00682.

Takahashi, H., Taylor, M.J., Sobral, J.H.A., Medeiros, A.F., Gobbi, D., Santana, D.C., 2001. Fine structure of the ionospheric plasma bubbles observed by the OI 6300 and 5577 airglow images. Adv. Space Res. 27 (6–7), 1189–1194. https://doi.org/10.1016/S0273-1177(01)00159-4.

Takahashi, H., Taylor, M.J., Pautet, P.-D., Medeiros, A.F., Gobbi, D., Wrasse, C.M., et al., 2009. Simultaneous observation of ionospheric plasma bubbles and mesospheric gravity waves during the SpreadFEx Campaign. Ann. Geophys. 27, 1477–1487. https://doi.org/10.5194/angeo-27-1477-2009.

Takahashi, H., Essien, P., Figueiredo, C.A.O.B., Wrasse, C.M., Barros, D., Abdu, M.A., Otsuka, Y., Shiokawa, K., Li, G., 2021. Multi-instrument study of longitudinal wave structures for plasma bubble seeding in the equatorial ionosphere. Earth Planet. Phys. 5 (5), 368–377. https://doi.org/10.26464/epp2021047.

Tsunoda, R.T., 1985. Control of the seasonal and longitudinal occurrence of scintillations by the longitudinal gradient in integrated *E* region Pedersen conductivity. J. Geophys. Res. 90 (A1), 447–456. https://doi.org/10.1029/JA090iA01p00447.

Tsunoda, R.T., Livingston, R.C., McClure, J.P., Hanson, W.B., 1982. Equatorial plasma bubbles: vertically elongated wedges from the bottomside F layer. J. Geophys. Res. 87 (A11), 9171–9180. https://doi.org/10.1029/JA087iA11p09171.

Vadas, S.L., Crowley, G., 2010. Sources of the traveling ionospheric disturbances observed by the ionospheric TIDDBIT sounder near Wallops Island on 30 October 2007. Journal of Geophysical Research: Space Physics, 115(A7). https://doi.org/10.1029/2009JA015053.

Woodman, R.F., La Hoz, C., 1976. Radar observations of F region equatorial irregularities. J. Geophys. Res. 81 (31), 5447–5466. https://doi.org/10.1029/JA081i031p05447.